# A REVIEW AND COMPARISON OF HYSTERESIS MODELS FOR MAGNETOSTRICTIVE MATERIALS

Sina Valadkhan, Department of Mechanical Engineering,
University of Waterloo, email: svaladkh@uwaterloo.ca
Kirsten Morris, Department of Applied Mathematics,
University of Waterloo, email: kmorris@birch.math.uwaterloo.ca
Amir Khajepour, Department of Mechanical engineering,
University of Waterloo, email: akhajepour@uwaterloo.ca

## ABSTRACT

The modeling of magnetization in magnetostrictive materials is studied. Magnetostrictive materials elongate in the presence of a magnetic field, and can be useful as actuators. These materials are highly nonlinear, and hence, difficult to control. Accurate models are important to the development of stabilizing controllers with good performance. Here, Terfenol-D, a magnetostrictive material is studied. A setup was designed to measure different parameters of a Terfenol-D sample. Using experimental data, the Preisach, homogenized energy, and Jiles-Atherton models are evaluated. For each model, the parameters are identified for Terfenol-D. The ease of use and accuracy of these models in the prediction of Terfenol-D behavior are compared.

## 1. INTRODUCTION

In recent years, a growing demand for micropositioning devices has been seen in industry. Micropositioning actuators are now commonly used in optical fiber alignment, biological cell micromanipulation, scanning microscopes and chip manufacturing. Currently, most of the micropositioning actuators are made of piezoceramic materials because of their fast response time and small hysteresis.

There are demands for actuators with more force, larger stroke and faster response. For this purpose, the possibility of using other active materials for actuation is being examined. Among possible choices, Terfenol-D is a competitive choice. Terfenol-D, a magnetostrictive material, is an alloy of iron, terbium and dysprosium. In comparison with other active materials, it has a very large force and displacement with a fast response time. By correctly considering eddy currents in the actuator design, Terfenol-D actuators can provide high-frequency responses up to 30 kHz.

In spite of its superior response, its application is less common in micropositioning devices. Terfenol-D, like other magnetic materials, has hysteresis. This nonlinearity and hysteresis makes it difficult to control. For this purpose, extensive research in hysteresis modeling is underway. Since in many micropositioning tasks, sub-micron accuracy is required, an accurate hysteresis model and control system is required if Terfenol-D is to be used for micropositioning applications.

The Preisach and Jiles-Atherton models are two of the most important hysteresis models for magnetostrictive materials. The Preisach model is one of the earliest hysteresis models. This phenomenological model was developed in 1935 for magnetic materials [1]. The Preisach model is explained in detail in [2]. In this model, the output is the weighted sum of the output of a continuum of hysteresis relays. The weight function for the relays depends on the material and needs to be identified. The Preisach model has been applied to many hysteretic systems, for example [3, 4]. Many variations of this model have been developed.

In [5], the homogenized energy model for magnetostrictive materials is introduced. This model has many similarities with the Preisach model. Unlike the Preisach model, this model is derived from a physical model for magnetic materials. The system equilibrium points are found by modeling the Helmholtz free energy for each dipole. This model has a weight function similar to the Preisach model which is determined by experimental data. In [5], the weight function is a Gaussian distribution with a few free parameters. In [6], this model was extended to a general weight function. This extension improves the accuracy of the model.

In [7], the Preisach model is combined with a linear system to develop a hysteresis model for Terfenol-D that includes dynamical effects. In this model, a general weight function is used with an iterative identification algorithm. Experimental data and model results are compared at different frequencies.

As stated before, the weight function for the Preisach and homogenized energy models depends on the system and must be identified with experimental data. Several identification algorithms have been proposed for this task. In [8], the identification problem is reformulated using a least-squares technique. In [6], this approach is examined in more detail for ferroelectric materials.

There are many implementations of the Jiles-Atherton model [9] for magnetostrictive materials. In the Jiles-Atherton model, the main magnetization mechanism is domain wall motion. Using an energy analysis, reversible and irreversible component of magnetization are modeled and a differential equation formulation for the system is obtained. This model has a few parameters to be identified. A major weakness of the Jiles-Atherton model is that it does not produce closed minor loops. Several corrections have been suggested to close the minor loops. This issue is fully discussed later in this paper.

In [10, 11], the Jiles-Atherton model is extended. It is suggested that the effects of stress for magnetostrictive materials can be represented with an additional magnetic field. In [11], the Jiles-Atherton model with quadratic magnetostriction is used. The effect of stress on magnetization is also modeled. The model results are compared with experimental data from a Terfenol-D sample.

The prime focus of this paper is evaluating hysteresis models for magnetostrictive materials in terms of accuracy in the presence of minor loops. Using experimental data,

the model parameters for the Preisach, homogenized energy, and Jiles-Atherton models are identified. The models are evaluated by comparing the model results with another set of experimental data.

The outline of this paper is as follows: In the next section, the test rig used to obtain experimental data is described. The experiments and data interpretation procedures are explained. It is shown that due to a relation between magnetization and elongation, the models only need to reproduce the magnetization. The Preisach model, its identification algorithm and model validation are included in Section 3. Section 4 covers the homogenized energy model and its identification and validation by experimental data. In Section 5, the Jiles-Atherton model and the algorithm used for proper minor loop handling are explained. The models are compared in the final section.

## 2. EXPERIMENTAL APPARATUS AND DATA COLLECTION

A test rig was designed to measure different parameters of Terfenol-D under different stresses and magnetic conditions. This test rig is shown in Figure 1. A Terfenol-D rod is surrounded by a magnetic coil in the actuation unit. The rod and coil are enclosed in a cylinder. An optical encoder with a resolution of 10nm measures the displacement produced by the actuation unit. A set of washer springs are used to load the actuation unit. The applied force is measured with a load cell and can be adjusted with a bolt on top of the setup. A frame made of aluminium is used to hold different parts of the setup together. Aluminium was chosen because of its neutral magnetic properties, resulting in no interference with magnetic components.

Terfenol-D cannot resist tension and should only be used in compression. This compression is supplied by the washer springs. The springs are soft enough to provide a constant compression force for different displacements produced by the actuation unit. The coil inside actuation unit is connected to a power supply controlled by a computer. There is a pickup coil in the actuation unit which measures the flux density inside the Terfenol-D rod. Two temperature sensors measure the coil and Terfenol-D rod temperature. The coil temperature is measured to make sure that it is not overheated and the Terfenol-D rod temperature is measured to compensate for any effects of thermal expansion by subtracting coefficient of thermal expansion times the temperature from the displacement. The coefficient of thermal expansion is measured at zero magnetization. It was observed that the temperature rise in each experiment is less than 1ºC and hence negligible. The current in the magnetic coil is measured in the power supply unit.

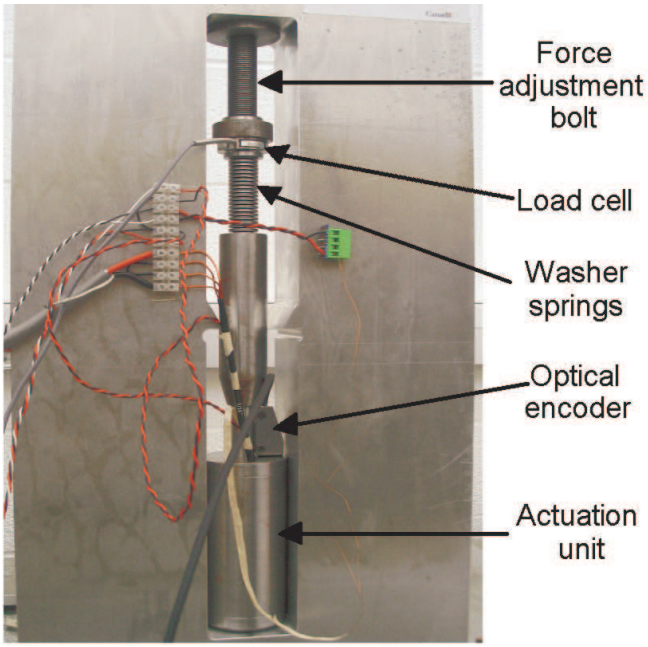


Figure 1: The experimental setup

This setup is used to obtain the relation between magnetic field *H* and magnetization *M* experimentally inside the Terfenol-D rod. The magnetic field *H* is controlled by the coil current and is considered to be the hysteretic system input. The magnetization *M* is a function of the magnetic field *H* and it is considered to be the output. Neither of these parameters is directly measurable.

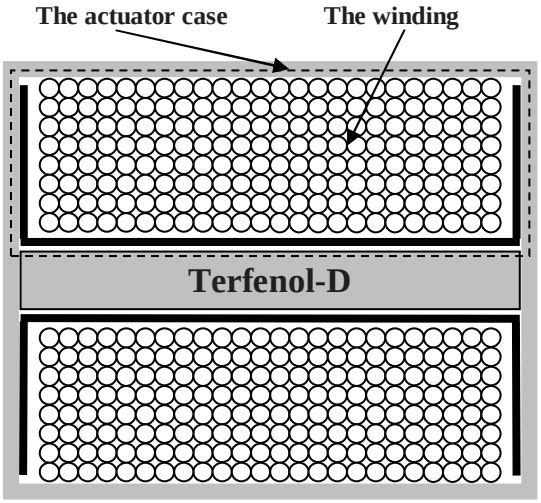


Figure 2: The magnetic circuit path.

To find the magnetic field *H*, the magnetic circuit for the actuation unit needs to be analyzed. Fig. 2 shows a cross-section of the actuation unit. The magnetic circuit path is

shown with dashed line. As shown in this figure, the magnetic circuit path goes through the Terfenol-D rod and is completed by the actuator case. Ampere's law for this magnetic circuit can be written as:

$$ni = \oint H.dl = \int_{case} H.dl + H_{TD} l \qquad (1)$$

where $l$ is the length of Terfenol-D rod, $H_{TD}$ is the magnetic field inside the Terfenol-D sample, $i$ is the electrical current and $n$ is the number of turns of the winding. If $\int_{case} H.dl$ is known, one can use equation (1) to compute the magnetic field $H$ inside the Terfenol-D rod. Since the flux density $B$ is measured by the pickup coil, the following equation can be used to compute magnetization $M$:

$$B = \mu_0 (H + M) . \qquad (2)$$

To find $\int_{case} H.dl$, the hysteresis relation for the actuator case must be known. A set of experiments was performed with the Terfenol-D rod replaced by a rod of cold rolled steel with known magnetic properties. In this case, Ampere's law can be written as:

$$ni = \oint H.dl = \int_{case} H.dl + H_{sample} l . \qquad (3)$$

Using the magnetic properties, $H_{sample}$ can be computed by looking up in the hysteresis curve. Now equation (3) can be used to obtain $\int_{case} H.dl$. It was found that $\int_{case} H.dl$ is small compared to $H_{TD}l$ (more than ten times smaller), that is, the computed magnetic field $H$ is only slightly modified if $\int_{case} H.dl$ is assumed to be zero.

When a magnetostrictive material is in a magnetic field $H$, in addition to magnetization, elongation is also seen. Both elongation and magnetization are also affected by the mechanical stress applied to the material. For most magnetostrictive materials under a constant stress, there exists a simple relation between magnetization $M$ and elongation $\lambda$. Fig. 3 shows the elongation versus magnetization for all experimental data when the stress is 7.18 MPa. It is seen that, ignoring experimental errors, an algebraic relation exists between the elongation $\lambda$ and $M$ which is independent of system history. The similarity between Fig. 3 and a parabola suggests that the function $\lambda(M)$ can be approximated by a polynomial function of even powers of $M$ [12]:

$$\lambda(M) = \gamma_2 M^2 + \gamma_4 M^4 + \cdots \qquad (4)$$

where parameters $\gamma_2$ and $\gamma_4$ depend only on stress. Usually the terms higher than $\gamma_4$ are not used. For the experimental data shown in Fig. 3, numerical values of $\gamma_2$ and $\gamma_4$ are: $\gamma_2 = 3.374\times10^{-15} (m/A)^2$ and $\gamma_4 = -1.9566\times10^{-27} (m/A)^4$. In Fig. 3, the curve given by equation (4) is shown with a dashed line. This dashed line lies among the experimental

data and cannot be clearly seen, which shows an excellent agreement between the curve and the experimental data. The relation $\lambda(M)=\gamma_2 M^2$ represents the magnetization-elongation relation with good accuracy. The elongation $\lambda$ is measured by an encoder and magnetization $M$ is obtained experimentally using equation (2).

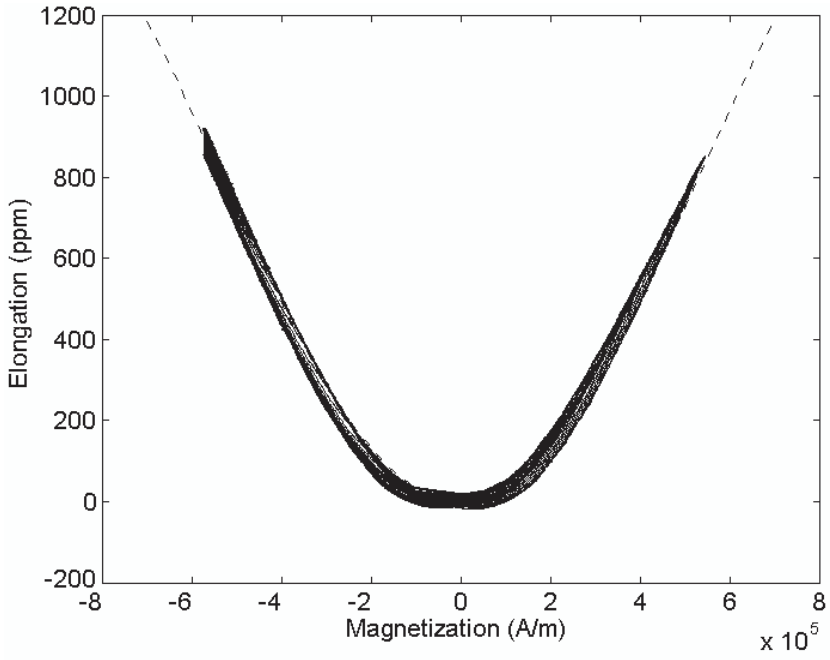


Figure 3: Elongation versus magnetization for Terfenol-D. The dashed curve is given by equation (4)

For magnetic materials, a hysteresis curve is a plot of magnetization versus magnetic field $H$. If the input is oscillating between the positive and negative saturation values for the material, the hysteresis curve is called the major loop, otherwise it is called a minor loop, especially if the curve is not symmetric about the origin. A first-order descending curve is a minor loop obtained when the input of the hysteretic system is between an arbitrary point and negative saturation of the material. For the Terfenol-D experiment, first-order descending curves are obtained for forty minor loops. These loops are shown in Fig. 4.

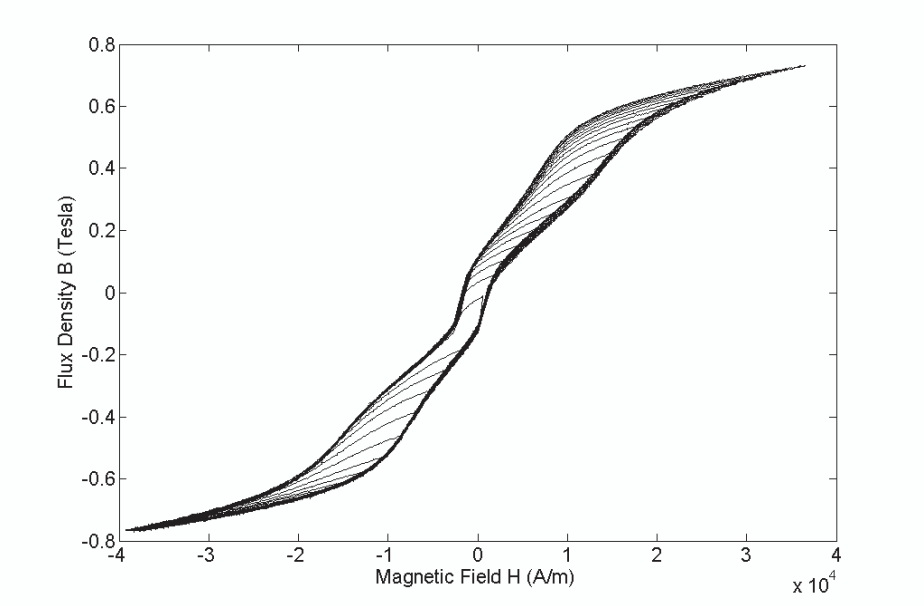

Figure 4: Experimental data for Terfenol-D.

One of the interesting aspects of Terfenol-D hysteresis is a twisted section in the middle of the hysteresis curve as shown in Fig. 4. This twisted section is not visible in the hysteresis curve of other magnetic materials. It is believed that this curvature is caused by multiple equilibrium points of the dipoles in the material.

In a magnetic material, there are a large number of magnetic dipoles. Each dipole contributes to the overall macroscopic magnetization. The dipoles cannot move, but are free to rotate in their place. There are several spatial directions which are preferable for the dipoles to other directions. Such a direction is called an easy axis.

For large positive and negative magnetic fields, the material is saturated. In these cases, the dipoles are mostly parallel to the applied magnetic field. If the magnetic field is brought from one saturated state to the other one, the dipoles do not change state in a single transition. There are multiple intermediate equilibrium points near easy axes. When the magnetic field is increased, a transition from an equilibrium point to another generates a sharp change in the magnetization. Between the transitions, the dipole leans toward the applied field when the field is increased and a slow change in the magnetization is seen. As a result, periods of sharp and slow changes in magnetization happen after another. As seen in Fig. 4, this results in a twisted portion in the middle of the hysteresis curve. For more information, see [13, 14].

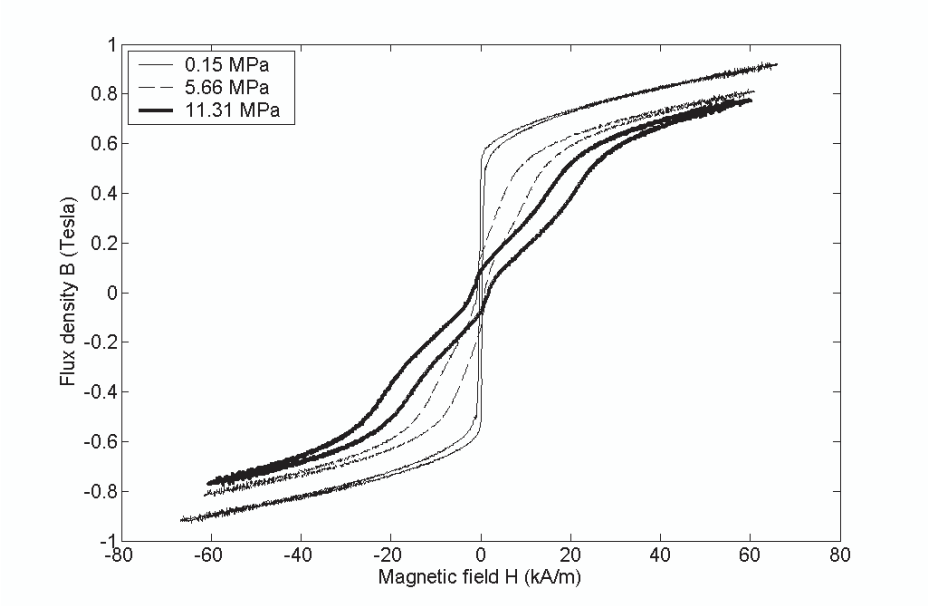


Figure 5: The major loop at different loads.

The hysteresis curves of Terfenol-D are significantly load-dependent. In Fig. 5, the major hysteresis loop at different stress levels are shown. It can be seen that at low loads, only a small amount of hysteresis is present. The twisted portion in the middle and the overall slope of the curve depend on the load. The load-dependence of Terfenol-D is not considered here.

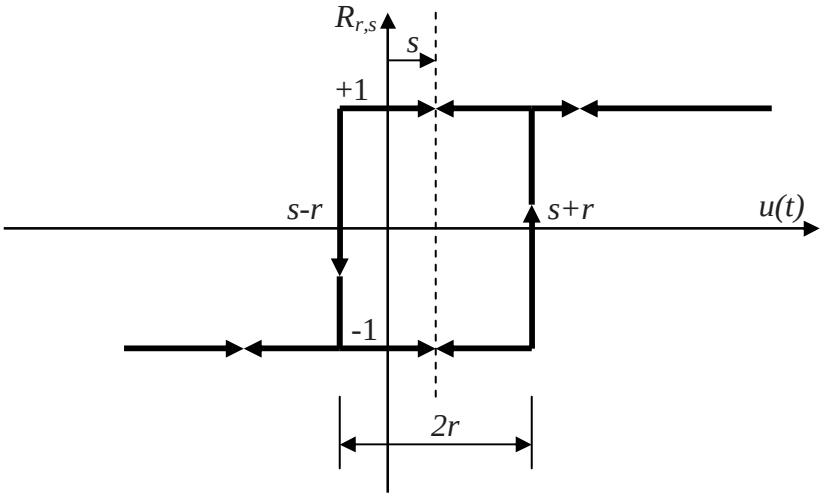


Figure 6: The Preisach relay.

## 3. THE PREISACH MODEL

The Preisach model [1] is the most common and probably the most important hysteresis model in the literature. This model is not based on any physical model of hysteretic materials and is phenomenological. It was developed about seventy years ago for magnetic materials.

In this model, the output is the weighted sum of the output of a continuum of hysteresis relays. The output of each relay can be either +1 or -1. In Fig. 6 a typical hysteresis relay is shown. Each relay is denoted by two parameters *r* and *s*.

The model output is:

$$y(t) = \int_0^\infty \int_{-\infty}^\infty R_{r,s}[u(\cdot)](t)\mu(r,s)dsdr \ . \qquad (5)$$

Here, *u(t)* is the input, $R_{r,s}$ is the output of the relay, *y(t)* is the model output and $\mu(r,s)$ is a weight function determined by experimental data.

The Preisach model is easier to understand with the introduction of Preisach plane. In the Preisach plane, the variable for horizontal axis is *r* and *s* for the vertical axis.

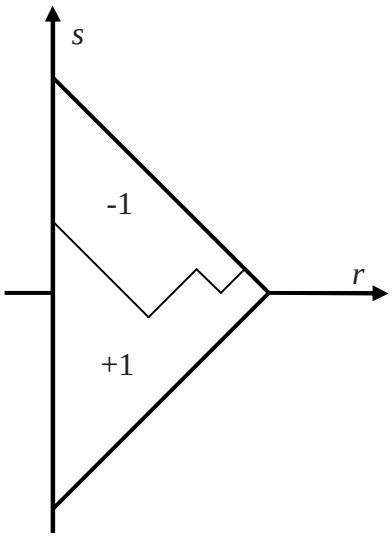


Figure 7: The Preisach plane.

Each point in this plane is in a one-to-one relation with a Preisach relay. Figure 7 shows the Preisach plane for a typical system. Because of physical reasons, the relays having large *r* or *s* values do not have a significant contribution to a change in the model output and their associated weight function is small. For simplicity, the relays outside the triangle in Fig. 7 are not considered and their weight function is assumed to be zero.

Each point inside the triangle in Fig. 7 represents a Preisach relay. The relays in +1 state are separated from the relays in -1 state with a broken line. The state of the system is represented with this broken line [15].

In order to use this model, the weight function $\mu(r,s)$ needs to be determined. There are two general approaches to this problem. A distribution for $\mu(r,s)$ with some free parameters can be assumed, and then the values for the parameters that best match modeled output and experimental data can be found. This approach is used for the homogenized energy model.

Alternatively, a general weight function can be used. It is assumed that $\mu(r,s)$ is piecewise constant. This means that the weight function is equal to a constant value $T_{m,n}$ in a small square defined by:

$$\begin{aligned} cm < s - r \le c(m+1) \\ cn < s + r \le c(n+1) \end{aligned} \qquad (6)$$

where $m$ and $n$ are integer parameters and c is a constant [16]. (See Fig. 8(c).) Using this approach, the model weight function is represented by a two dimensional matrix $T_{m,n}$. This reduces the number of model parameters to a finite number. Now the experimental data can be used to find a set of optimum values for these parameters.

Suppose that for a hysteretic system, a first-order descending curve between negative saturation and some input $cn$ is obtained. Define $\Delta_{cm,cn}$ to be the system output when the input is equal to $cm$ and the input is decreasing. The quantity $\Delta_{cm,cn}$ is obtained directly from experimental data. Fig. 8(a) shows the Preisach plane for this state. By comparing $\Delta_{cm,cn}$ and $\Delta_{c(m+1),cn}$ (Fig. 8(b)), it is seen that $\frac{1}{2}(\Delta_{c(m+1),cn} - \Delta_{cm,cn})$ is equal to the integral of the weight function $\mu(r,s)$ over the shaded area. Using a similar argument $\frac{1}{2}(\Delta_{c(m+1),c(n+1)} + \Delta_{cm,cn} - \Delta_{cm,c(n+1)} - \Delta_{c(m+1),cn})$ is equal to the integral of the weight function $\mu(r,s)$ over the square defined by equation (6) and shown in Fig. 8(c). Since the weight function is assumed to be constant in this region, this relation yields a solution for $T_{m,n}$ which is the weight function in the square denoted by $m$ and $n$:

$$T_{m,n} = \frac{1}{2c^2}(\Delta_{c(m+1),c(n+1)} + \Delta_{cm,cn} - \Delta_{cm,c(n+1)} - \Delta_{c(m+1),cn}). \qquad (7)$$

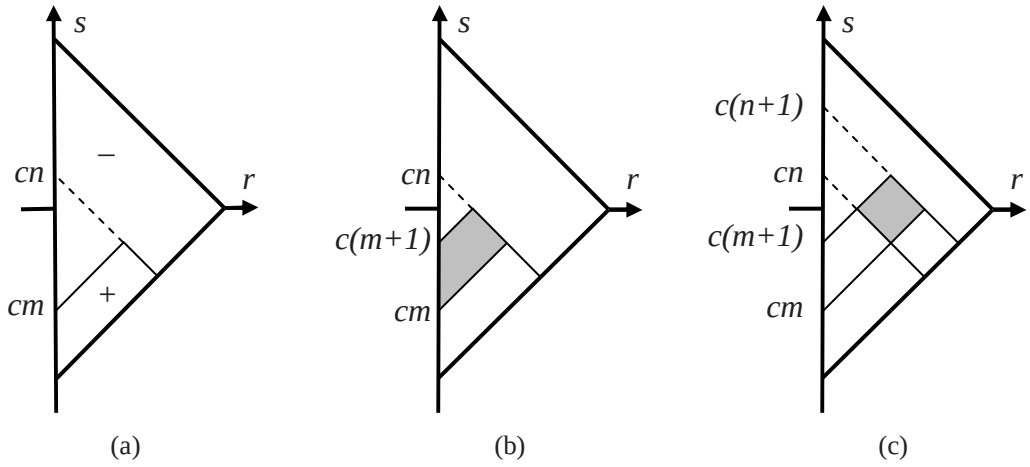


Figure 8: The Preisach plane for a first-order descending curve.

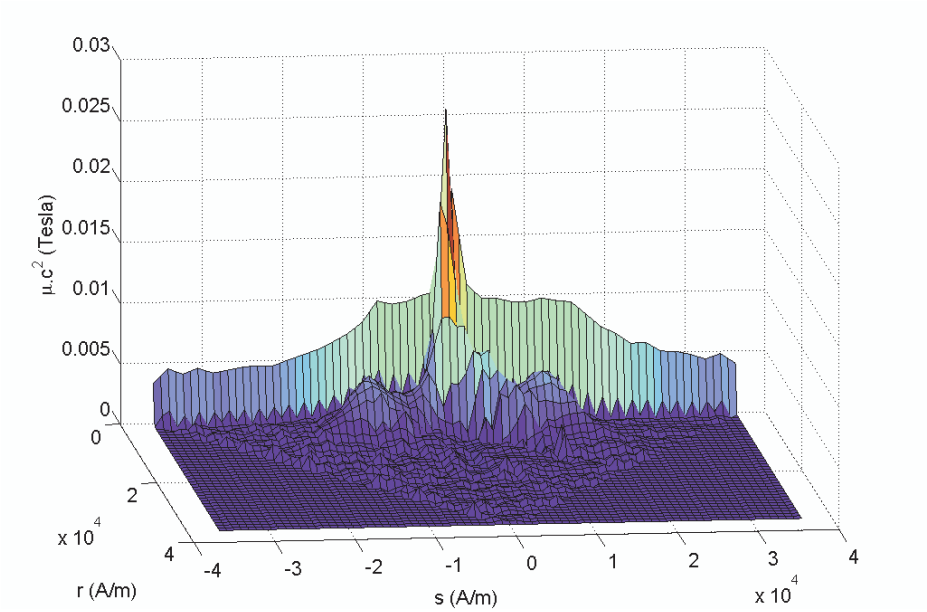


Figure 9: The Preisach weight function.

As stated before, $\Delta_{cm,cn}$ is directly obtained from experimental data. Using equation (7), $T_{m,n}$ or the weight function $\mu(r,s)$ in each cell can be obtained. Fig. 9 displays the identified weight function $\mu(r,s)$ for the Terfenol-D sample. To verify if the Preisach model with this weight function can predict Terfenol-D behaviour accurately, an additional experiment on Terfenol-D was performed. In the beginning of this experiment, the input is oscillating between negative and positive saturation values. The amplitude of the input is decreased gradually and finally the input settles down to zero.

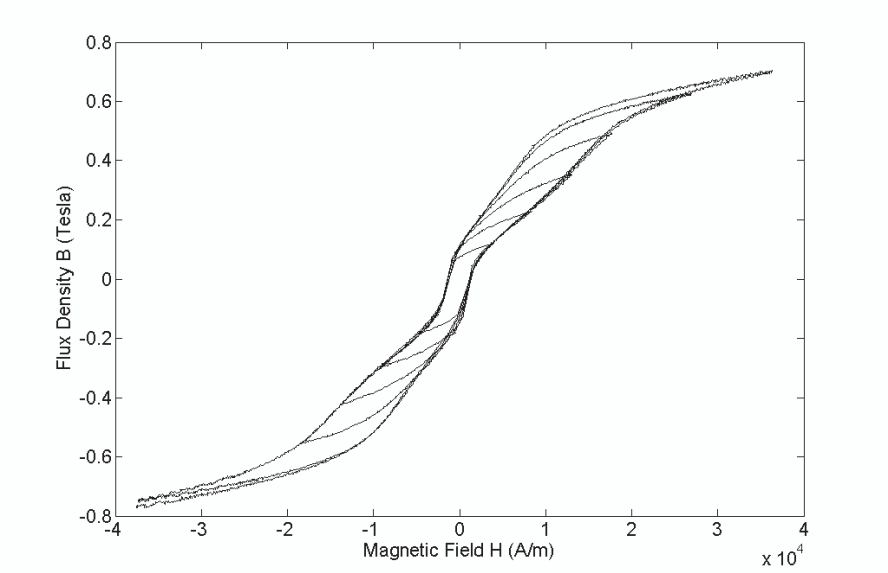


Figure 10: Experimental data for the second experiment.

Fig. 10 shows the actual output versus input for this experiment and Fig. 11 shows the Preisach model output for the same input. It is seen that the experimental data and model results are very similar, which shows the accuracy of the Preisach model prediction. The special curvature of Terfenol-D hysteresis curve is completely captured and reproduced.

The major loop of the initial experimental data and the second experiment are not identical. Small variation of experimental parameters is likely the reason for this difference. This is believed to be the main source of error.

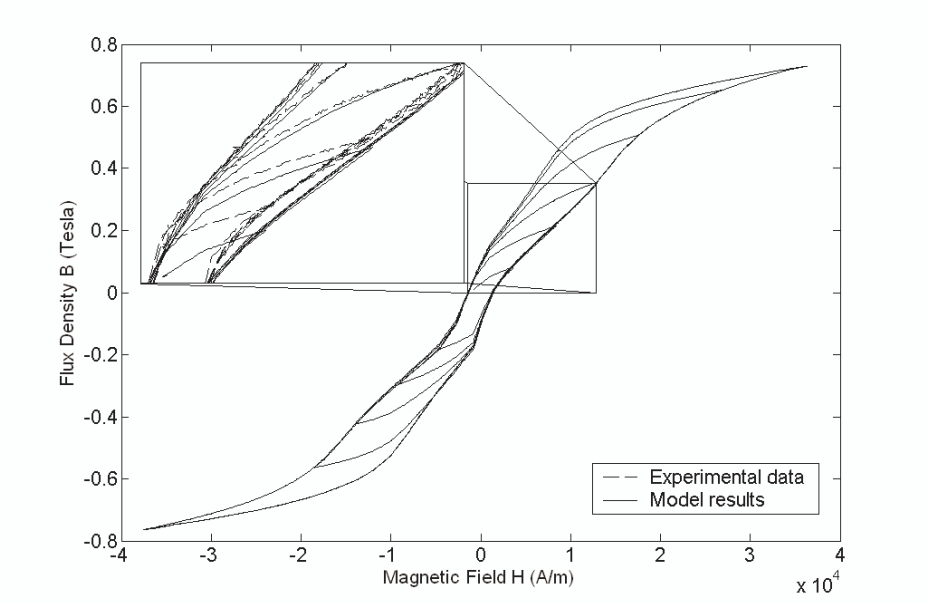


Figure 11: The Preisach model results for the second experiment.

## 4. THE HOMOGENIZED ENERGY MODEL

In the homogenized energy model [5], a physical model for magnetostrictive materials is used to develop a hysteresis model. The material is assumed to be composed of a large number of weakly interacting dipoles. For each dipole, the Helmholtz free energy is modeled. The equilibrium points of the dipole are found by minimizing the Gibbs energy. Similar to the Preisach model, two equilibrium states are found for each dipole. Each dipole is denoted by two parameters: the coercive field $H_c$ which is similar to $r$ for the Preisach relay in Fig. 6 and the interaction field $H_I$ which is similar to $s$.

Unlike the Preisach model, a transition between the equilibrium points for the dipole is possible when the input is constant due to thermal relaxation. In this case, the magnetization can change when a constant magnetic field is applied. Thermal relaxation effects are reported for steel samples [17].

In this series of experiments with Terfenol-D, thermal relaxation was not observed. Fig. 12 shows the magnetic field and magnetization versus time. It is seen that the magnetization is only changing when the magnetic field is changed. Similar results are obtained for other values of magnetic field and magnetization.

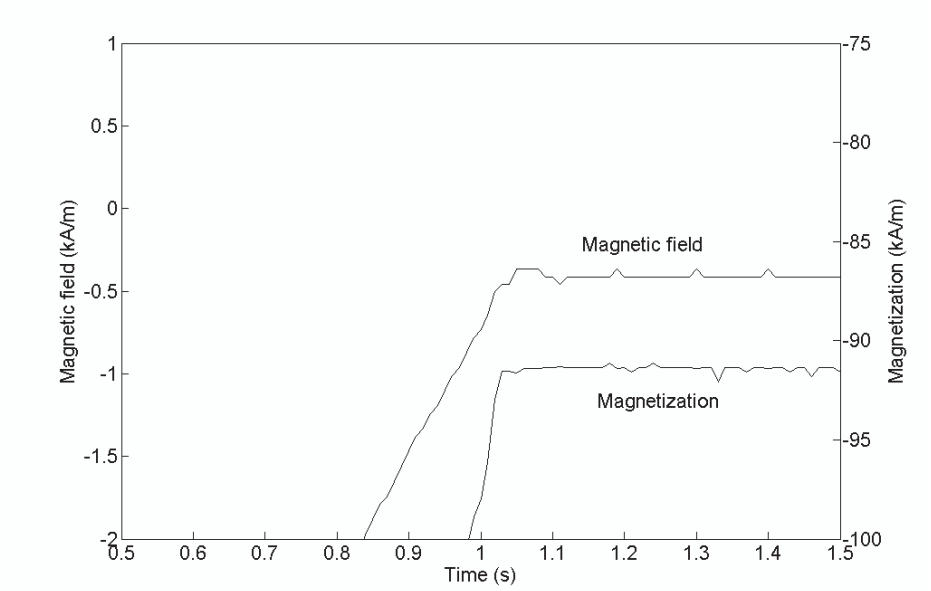


Figure 12: Magnetic field and magnetization versus time.

In the absence of thermal relaxation, the transitions between the equilibrium points for a dipole are similar to the transitions of a Preisach relay, as shown in Fig. 6. In this situation, the equilibrium magnetization for each dipole $\overline{M}$ is:

$$\overline{M}(H, H_I, H_c) = \frac{H + H_I + R_{H_c,H_I}(H) M_R \eta}{\eta - \dfrac{2Y\gamma_2 \varepsilon}{\mu_0}}. \qquad (8)$$

In this equation, $\eta$ and $M_R$ are model parameters, $Y$ is the Young modulus for the material, $\varepsilon$ is strain and $R$ is the Preisach relay defined in the previous section. It is assumed that the second term in equation (4) can be ignored and $\lambda(M) = \gamma_2 M^2$. In this case, the strain $\varepsilon$ is given by the following equation:

$$\varepsilon = \frac{\sigma}{Y} + \gamma_2 M^2 \qquad (9)$$

where $\sigma$ is the stress.

Because of crystal imperfections and impurities, the dipoles are not exactly similar. By assuming a distribution $\mu(H_c,H_I)$ for the dipoles, the overall magnetization $M$ can be computed:

$$M = \int_0^\infty \int_{-\infty}^\infty \overline{M}(H, H_I, H_c) \mu(H_c, H_I) dH_I dH_c \qquad (10)$$

By combining equations (8) and (10), the following result is obtained.

$$M = \frac{1}{\eta - \dfrac{2Y\gamma_2 \varepsilon}{\mu_0}} \Bigg[ H \int_0^\infty \int_{-\infty}^\infty \mu(H_c, H_I) dH_I dH_c + \int_0^\infty \int_{-\infty}^\infty H_I \mu(H_c, H_I) dH_I dH_c + M_R \eta \int_0^\infty \int_{-\infty}^\infty R_{H_c,H_I} \mu(H_c, H_I) dH_I dH_c \Bigg]. \qquad (11)$$

In this equation, the first term in the brackets is proportional to $H$, the second term is a constant, and the third term is similar to a Preisach model. This shows that there is a close connection between the Preisach model and the homogenized energy model in the absence of thermal relaxation. In fact, as $\eta$ approaches infinity, the homogenized energy model simplifies to the Preisach model.

Unlike the Preisach model, the magnetization given by equation (11) depends on strain $\varepsilon$. The homogenized energy model is based on a physical model for the material. Because of this physical basis, features like thermal relaxation and load dependence can be incorporated into the model.

Similar to the Preisach model, a weight function $\mu(r,s)$ is needed. For the homogenized energy model, a Gaussian [5], log normal [18], and general [6] weight functions are used.

$$\text{Gaussian}: \quad \mu(r,s) = Ce^{-\frac{H_I^2}{\bar{b}}} e^{-\frac{(H_c-\overline{H_c})^2}{b}}$$
$$\text{Log normal}: \quad \mu(r,s) = Ce^{-\frac{H_I^2}{\bar{b}}} e^{-\frac{\left(\ln\left(\frac{H_c}{\overline{H_c}}\right)\right)^2}{b}} \tag{12}$$

The parameters $b, \bar{b}, \overline{H_c}$, and $C$ are constant parameters. A general weight function can be implemented by using a piecewise constant function similar to the previous section.

Root-mean-square error was computed as follows: For each value of magnetic field $H$, error is computed by subtracting model results from experimental data. Total model error is computed by taking the root-mean-square of these errors.

For the Gaussian and log normal distributions, the best value for model parameters are found by numerically minimizing the root-mean-square error using Nelder-Mead simplex direct search method. The results are summarized in Table 1.

| Parameter | Gaussian distribution | Log normal distribution |
|---|---|---|
| $\eta$ | 17.766 | 0.47537 |
| $b$ | $1.1591\times10^{9}\ (A/m)^2$ | 10.837 |
| $\bar{b}$ | $2.2540\times10^{8}\ (A/m)^2$ | $1.4567\times10^{8}\ (A/m)^2$ |
| $\overline{H_c}$ | $-136030\ A/m$ | $\overline{H_c} = 0.81725\ A/m$ |
| $M_R$ | $7417.7\ A/m$ | $8.0029\times10^{5}\ A/m$ |
| $C$ | $2.0996\ (m/A)^2$ | $5.5034\times10^{-7}\ (m/A)^2$ |

Table 1: The model parameters for Gaussian and log normal distributions.

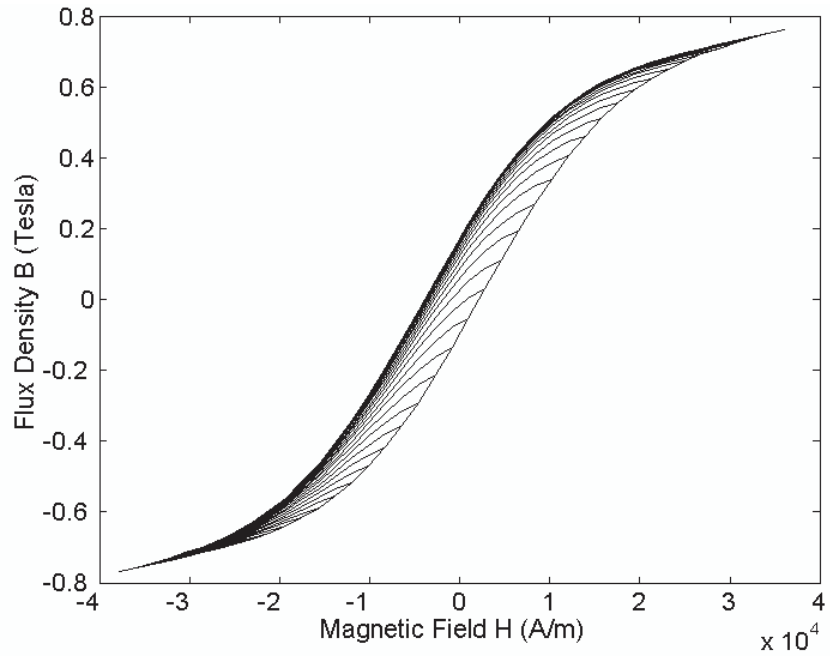

Figure 13: Minor loops produced by the homogenized energy model with a Gaussian distribution.

In Fig. 13, minor loops produced by this model are shown and Fig. 14 compares the model results and experimental data for a Gaussian distribution. It is seen that the model and experimental data are close, but the curvature in the middle is not accurately captured. In Fig. 15, the model results and experimental data are compared for a log normal distribution. The results for a log normal distribution are very similar to that of the Gaussian distribution. The experimental data shown in Figs. 14 and 15 is not used for model identification.

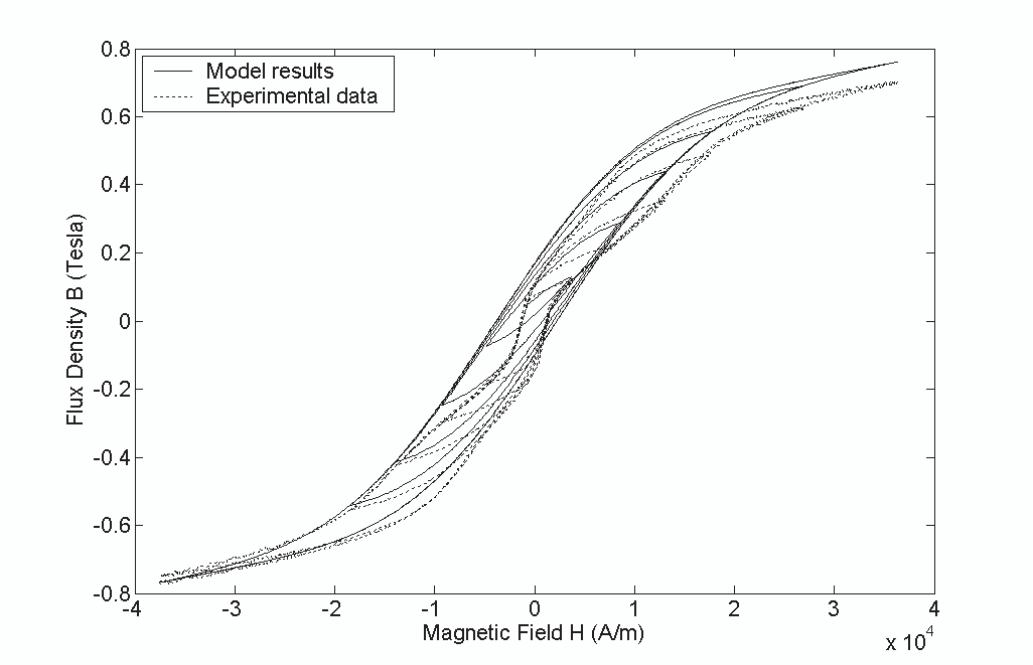


(a)

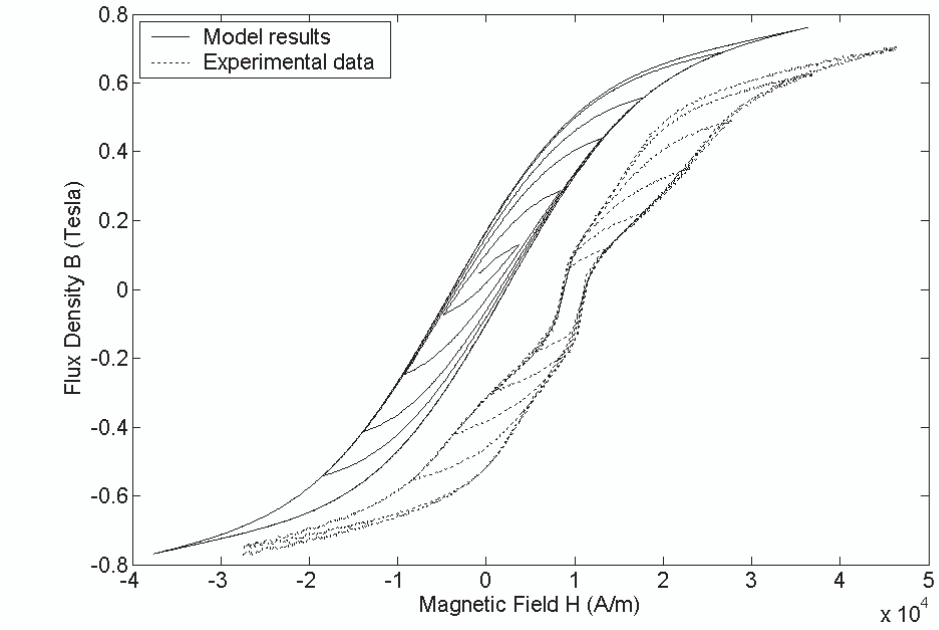


(b)

Figure 14: (a) The experimental data and the homogenized energy model results with Gaussian distribution. (b) The experimental results are shifted for easier comparison. The model was unable to reproduce the middle of the curve correctly.

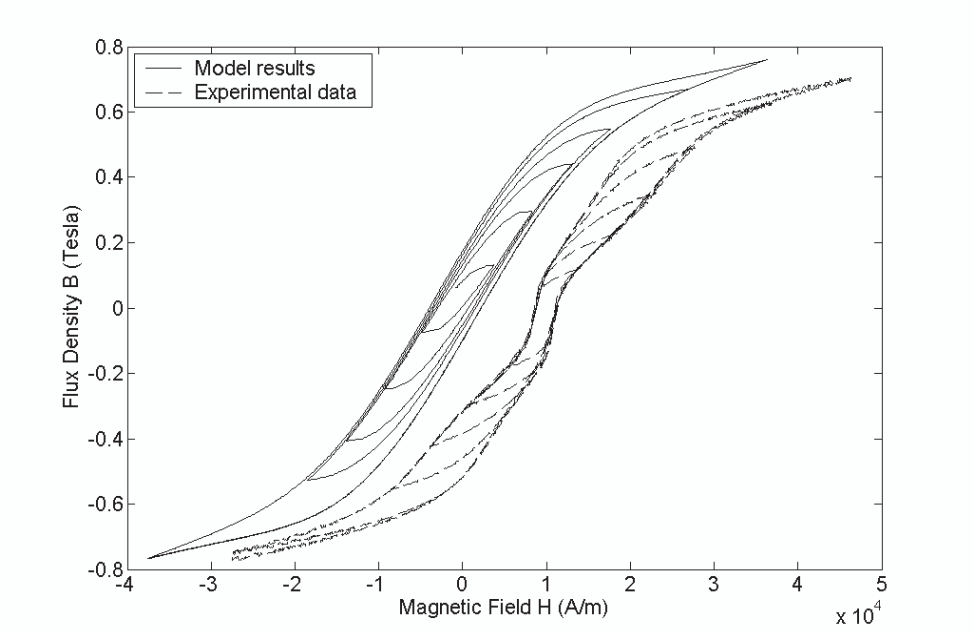


Figure 15: The experimental data and the homogenized energy model results with log normal distribution. The experimental results are shifted for easier comparison. The results are similar to that of the Gaussian distribution.

By using equations (7) and (11), the homogenized energy model with a general weight function can be identified. Equation (11) relates the homogenized energy model to the Preisach model. Using equation (7) and an argument similar to the previous section, the weight function is identified. It is shown in Fig. 16.

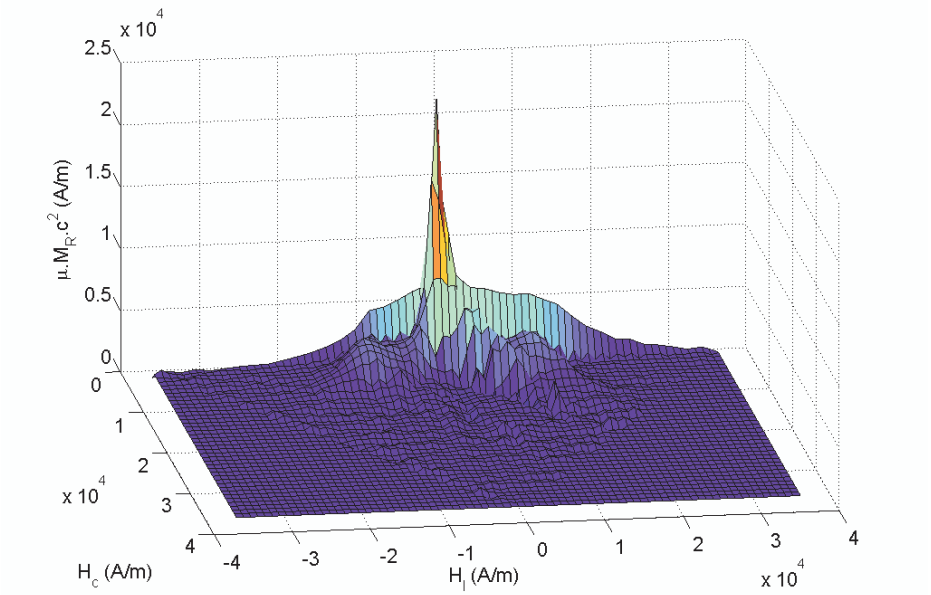


Figure 16: The general weight function for the homogenized energy model.

For a general weight function, the number of model parameters is much more than that for a Gaussian or log normal distribution. The identification problem has multiple solutions. To provide a unique solution, similar to [6], the parameter $\eta$ is chosen to match the hysteresis curve slope at saturation. It is also assumed that the distribution for the dipoles $\mu(H_c,H_I)$ is normalized.

$$\int_0^{\infty}\int_{-\infty}^{\infty}\mu(H_c,H_I)dH_I dH_c = 1 \qquad (13)$$

For the homogenized energy model with a general weight function, $\eta = 0.66$ and $M_R = 4.2769\times10^5 \ A/m$.

Similar to the previous section, the model results and unseen experimental data are compared. Hysteresis curves produced by the homogenized energy model with general weigh function are identical to those of the Preisach model in Fig. 11. The experimental data, including the twisted portion of the hysteresis curve is reproduced accurately.

## 5. THE JILES-ATHERTON MODEL

The following equations describe the Jiles-Atherton model [9]:

$$\frac{dM_{irr}}{dH} = \frac{(M_{an}-M_{irr})}{\delta k-\alpha(M_{an}-M_{irr})} \qquad (14)$$
$$M_{rev} = c(M_{an}-M)$$

where $c$, $\alpha$ and $k$ are model parameters, $M_{irr}$ and $M_{rev}$ are the irreversible and reversible components of magnetization, respectively; and $M_{rev} + M_{irr} = M$. Parameter $\delta$ is equal to +1 when $H$ is increased and -1 when $H$ is decreased. The parameter $M_{an}$ is the anhysteretic magnetization. For this model, the Langevin equation is used for the anhysteretic magnetization:

$$M_{an}(H_e) = M_s\left[\coth\left(\frac{H_e}{a}\right)-\frac{a}{H_e}\right] \qquad (15)$$

where $a$ and $M_s$ are model parameters and $H_e = H + \alpha M$.

It is seen that, in some cases, the magnetization computed by this model is increased when $H$ is decreased, which means negative differential susceptibility. This behaviour is not physical [19]. In [19], it is suggested that in this case, $\frac{dM_{irr}}{dH}$ should be set to zero.

Some minor loops, especially small minor loops near saturation, are not produced correctly by this model. In Fig. 17, curve A is a portion of an ascending major loop. If the input is slightly decreased (Curve B) and then increased again (Curve C), the produced minor loop will not be closed. This behaviour is unphysical. To correct this problem, a solution is suggested in [20]. Define:

$$\begin{aligned} \nu_f &= \frac{M_{irr}(H_+) - M_{irr}(H_-)}{\int_{H_-}^{H_+} \frac{M_{an} - M_{irr}}{\delta k - \alpha(M_{an} - M_{irr})} dH} \\ \nu'_f &= \frac{M_{rev}(H_+) - M_{rev}(H_-)}{\int_{H_-}^{H_+} c(\frac{dM_{an}}{dH} - \frac{dM_{irr}}{dH}) dH} \end{aligned} \qquad (16)$$

where $H_+$ and $H_-$ are the maximum and minimum value of magnetic field $H$ in the minor loop, respectively. In [20], it is suggested that equations (14) should be replaced by the following equations:

$$\begin{aligned} \frac{dM_{irr}}{dH} &= \nu_f \frac{(M_{an} - M_{irr})}{\delta k - \alpha(M_{an} - M_{irr})} \\ \frac{dM_{rev}}{dH} &= \nu'_f c(\frac{dM_{an}}{dH} - \frac{dM_{irr}}{dH}). \end{aligned} \qquad (17)$$

As seen in equation (16), $\nu_f$ and $\nu'_f$ are functions of $H_+$ and $H_-$, the starting and ending points of the major loop. As a result, this correction can be applied only if the ending point for the minor loop is known in advance. If the ending point is not known in advance, for example in real-time control, this correction cannot be used.

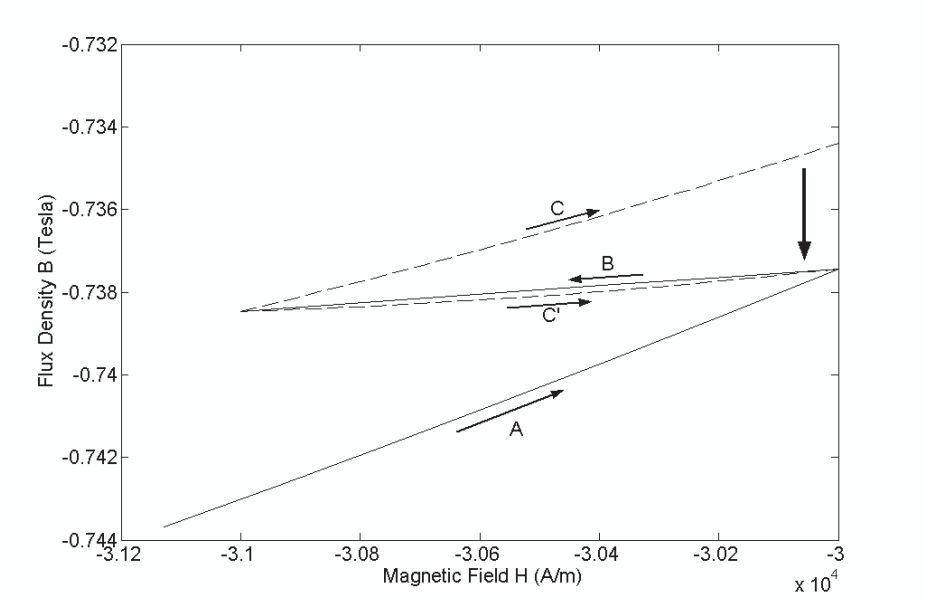


Figure 17: The closure of minor loops.

Unfortunately, equations (16) and (17) do not yield a fast algorithm. Equations (16) and (17) are nonlinear equations that need to be solved simultaneously. This algorithm is computationally expensive.

Scaling the hysteresis curve is another method for producing closed minor loops [21]. Here, each branch is scaled vertically to produce a closed loop. For example in Fig. 17, branch C is replaced by branch C'. Similar to the solution proposed in [20], the scaling is done separately for the reversible and irreversible components of magnetization. Since the scaling is computationally trivial and yields an efficient solution for closing the minor loops, it is used in this paper.

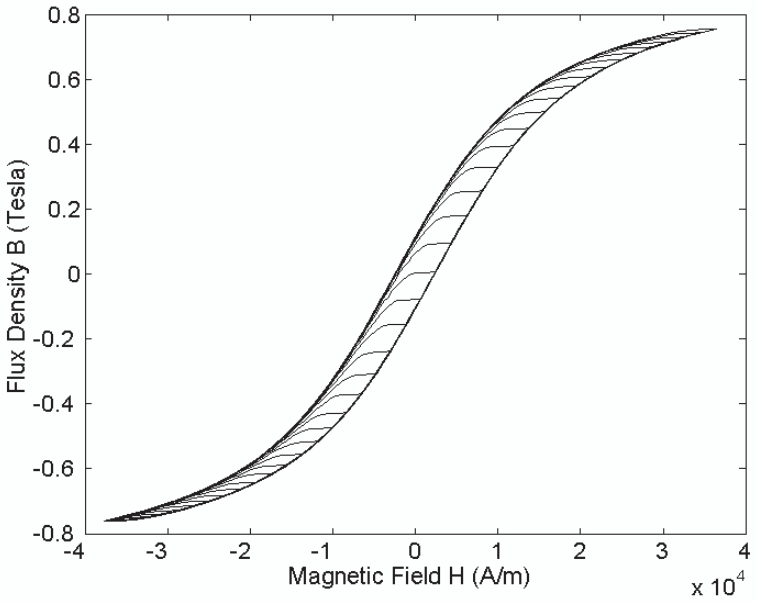

Figure 18: The minor loops produced by the Jiles-Atherton model.

The model parameters for the Jiles-Atherton model are identified using an algorithm similar to the algorithm used for the homogenized energy model for Gaussian and log normal distributions. The optimum model parameters are listed in Table 2.

| Parameter | $\alpha$ | $a$ | $M_s$ | $k$ | $c$ |
|---|---|---|---|---|---|
| Unit | 1 | $A/m$ | $A/m$ | $A/m$ | 1 |
| Value | $1.9903\times10^{-8}$ | 6200.2 | 690380 | 2476.6 | $5.7080\times10^{-4}$ |

Table 2: The Jiles-Atherton model parameters

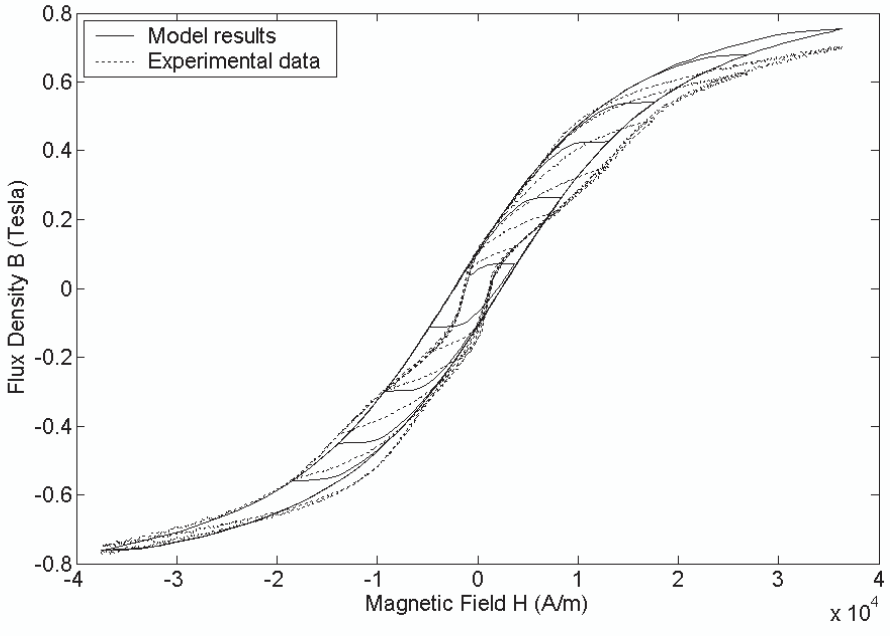


(a)

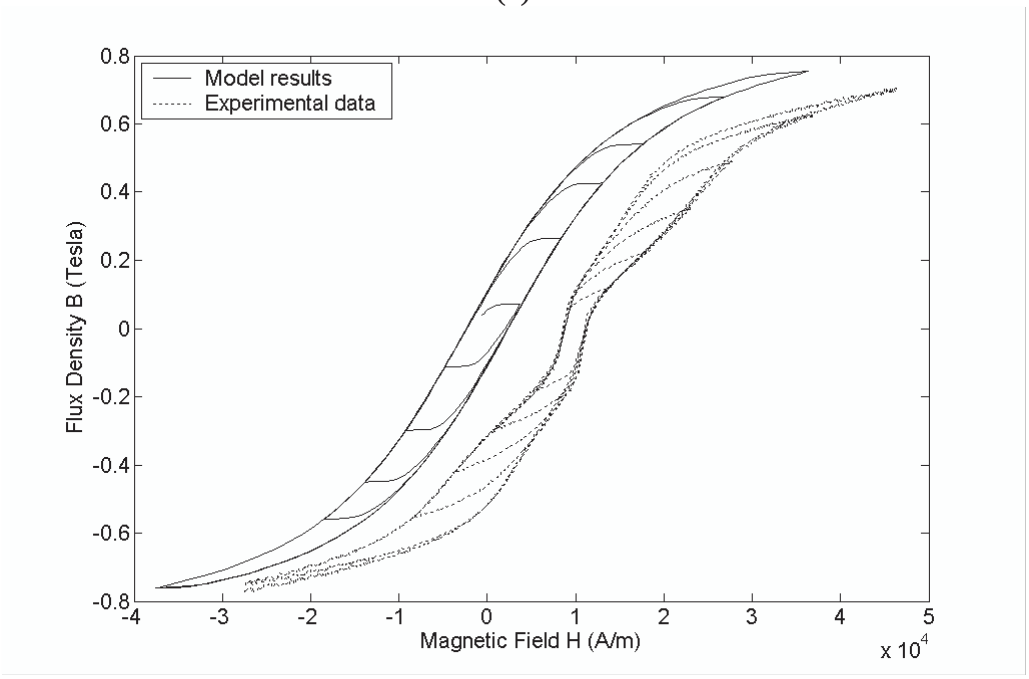


(b)

Figure 19: (a) The experimental data and the Jiles-Atherton model results. (b) The experimental results are shifted for easier comparison. The model was unable to reproduce the middle of the curve correctly.

In Fig. 18, the minor loops produced by this model are shown. Experimental data and model results are compared in Fig. 19. Similar to the homogenized energy model with a

Gaussian or log normal distribution, the model is close to the experimental data, but the twisted section of the experimental data is not captured.

## 6. CONCLUSIONS

For all of the models discussed in this paper, experimental data is needed for model identification. The data required is different for each model. The Preisach model and the homogenized energy model with a general weight function need at least a set of first-order descending curves. For the homogenized energy model with a Gaussian or log normal distribution and the Jiles-Atherton model, since they have only a few free parameters, a single loop is sufficient; for example the major loop.

The Preisach model and the homogenized energy model with a general weight function are similar in terms of accuracy. Both models could reproduce the experimental data with least error. The homogenized energy model with Gaussian or log normal distributions and the Jiles-Atherton model had about the same accuracy; and could not capture the twisted section in the middle of the hysteresis curve.

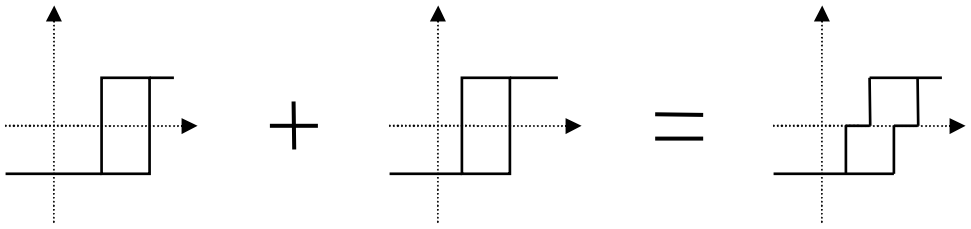

Figure 20: By combining two binary relays, a relay with an intermediate state is obtained.

As stated before, the twisted section is caused by intermediate equilibrium points near easy axes. Both Preisach and homogenized energy models assume only a binary state for the dipole. Surprisingly, both models are capable of reproducing the twisted portion accurately. By assuming that more than one hysteresis relay is used to represent each dipole, as illustrated in Fig. 20, a dipole with intermediate equilibrium states can be represented by binary hysteresis relays.

The Preisach model and the homogenized energy model with a general weight function have enough model parameters to accurately represent dipoles with intermediate equilibrium points with multiple hysteresis relays and hence, reproduce the experimental data accurately. The homogenized energy model with a Gaussian or log normal distribution is less flexible and cannot represent the dipoles accurately. As a result, the twisted section is not captured.

Simulations and identifications were run on a Pentium III ® 700 MHz with 384 MB of memory, using Matlab ®. In Table 3, the model comparison is summarized. Fitting error is the root-mean square error with respect to the experimental data set used for model identification. Prediction error is the accuracy of the predicted output for the unseen experimental data. Note that the calculations were not optimized and these timings are presented for comparison purposes only.

The identification of the Preisach model and the homogenized energy model with a general weight function were the fastest. The homogenized energy model with a Gaussian or log normal distribution and the Jiles-Atherton model were slower because of their iterative identification algorithm. The numerical optimization routine used needs up to 10,000 iterations for convergence. This leads to an identification time of several hours. The identification of the homogenized energy model with a Gaussian or log normal distribution was faster, because of an efficient algorithm.

Minor loops have a special importance in control applications. In a typical control system, usually the major loop is not experienced. For example, often the input oscillates about an operating point. In this case, a minor loop near that point is experienced. If the oscillation amplitude decays with time, complex nested loops may be produced. For this reason, it is important to have a hysteresis model capable of handling complex minor loops for control applications. The Preisach and homogenized energy models can handle minor loops properly. The minor loop handling for the Jiles-Atherton model is not done correctly for complex cases. If Figs. 11, 14 and 19 are compared, it is seen that the minor loops for the Jiles-Atherton model join the major loop faster than the experimental data. In contrast, for the homogenized energy model with a Gaussian or log normal distribution, the minor loops join the major loop much slower than the experimental data. It can be said that the Jiles-Atherton model underestimates the amount of input variation required to forget past history and the homogenized energy model with a Gaussian or log normal distribution overestimates this amount. The Preisach model and the homogenized energy model with a general weight function are the most accurate in this matter.

| **Parameter** | **Preisach model** | **Homogenized energy model (Gaussian)** | **Homogenized energy model (log normal)** | **Homogenized energy model (general)** | **Jiles-Atherton model** |
|---|---|---|---|---|---|
| Fitting error (Tesla) | 0 | 0.0356 | 0.0322 | 0 | 0.0254 |
| Prediction error (Tesla) | 0.0172 | 0.0569 | 0.0562 | 0.0177 | 0.0426 |
| Identification time | 3.1 s | ~1 hour | ~1 hour | 5.8 s | ~10 hours |
| Reproduction time | 1.5 s | 6.1 s | 6.1 s | 3.3 s | 1.3 s |
| Number of model parameters | 820 | 6 | 6 | 822 | 5 |
| Minor loop handling | √ | √ | √ | √ | × |

Table 3: Summary

The Preisach model and the homogenized energy model with a general weight function have more than 800 parameters to describe the material. This number is six for the homogenized energy model with a Gaussian or log normal distribution and five for the Jiles-Atherton model. The accuracy of the Preisach model and the homogenized energy model with a general weight function is partially due to the large number of parameters. Where high accuracy is crucial, these models are the best. The Jiles-Atherton model and homogenized energy model with a Gaussian or log normal distribution had similar accuracy and required similar number of parameters. However, the Jiles-Atherton model does not handle minor loops properly.

REFERENCES


1. Preisach, F., "Uber die magnetische nachwirkung", Zeitschrift fur Physik, vol. 94, 1935, pp. 277-302.
2. Mayergoyz, I., "Mathematical Models of Hysteresis and Their Applications", Elsevier Academic Press, Amsterdam, Boston, 2003.
3. Ktena, A., Fotiadis, D.I., Berger, A., Massalas, C.V., "Preisach Modeling of AFC Magnetic Recording Media", IEEE Transactions on Magnetics, Vol. 40, No. 4, July 2004, pp.2128-2130.
4. Gorbet, R.B., Wang, D.W.L., Morris, K.A., "Preisach model identification of a two-wire SMA actuator," Proceedings, IEEE international conference on robotics and automation, Vol. 3, 1998, pp. 2161-2167.
5. Smith, R.C., Dapino, M.J., Seelecke, S., "Free energy model for hysteresis in magnetostrictive transducers", Journal of Applied Physics, vol. 93, No. 1, 1 January 2003, pp. 458-466.
6. Smith, R.C., Hatch, A.G., Mukherjee, B., Liu, S., "A Homogenized Energy Model for Hysteresis in Ferroelectric Materials: General Density Formulation", Journal of intelligent material systems and structures, Vol. 16, No. 9, September 2005, pp. 713-732.
7. Tan, X., Barasa, J.S., "Modeling and control of hysteresis in magnetostrictive actuators", Automatica, Vol. 40, No. 9, September 2004, pp. 1469-1480.
8. Smith, R.C., Hatch, A.G., "Parameter estimation techniques for a class of nonlinear hysteresis models", Inverse problems, Vol. 21, No. 4, August 2005, pp. 1363-1377.
9. Jiles, D.C., Atherton, D.L., "Theory of ferromagnetic hysteresis", Journal of Magnetism and Magnetic Materials, vol. 61, 1986, pp. 48-60.
10. Sablik, M.J., Jiles, D.C., "Coupled Magnetoelastic Theory of Magnetic and Magnetostrictive Hysteresis", IEEE Transactions on Magnetics, vol. 29, No. 3, July 1993, pp. 2113-2123.
11. Dapino, M.J., Smith, R.C., Faidley, L.E., Flatau, A.B., "A Coupled Structural-Magnetic Strain and Stress Model for Magnetostrictive Transducers", Journal of Intelligent Material Systems and Structures, Vol. 11, February 2000, pp. 135-152.

12. Jiles, D.C., "Theory of the magnetomechanical effect", Journal of Physics D: Applied Physics, vol. 28, No. 8, 14 August 1995, pp. 1537-1546.
13. Clark, A.E., Teter, J.P., McMasters, O.D., "Magnetostriction jumps in twinned $Tb_{0.3}Dy_{0.7}Fe_{1.9}$," Journal of applied physics, Vol. 63, April 1988, pp. 3910-3912.
14. Armstrong, W.D., "An incremental theory of magneto-elastic hysteresis in pseudo-cubic ferro-magnetostrictive alloys," Journal of magnetism and magnetic materials, Vol. 263, 2003, pp. 208-218.
15. Gorbet, R.B., Morris, K.A., Wang, D.W.L., "Control of hysteretic systems: A state-space approach", *Learning, control and hybrid systems*, Edited by Yutaka Yamamoto, Shinji Hara, Bruce A. Francis and M. Vidyasagar, Springer-Verlag, New York, 1998, pp. 432-451.
16. Valadkhan, S., *Modeling of magnetostrictive materials*, MASc. Thesis, University of Waterloo, Department of Mechanical Engineering, 2004, pp. 86-91.
17. Braun, T.B., Smith, R.C., Dapino, M.J., "Experimental validation of a homogenized energy model for magnetic after-effects," Applied physics letters, Vol. 88, 122511, 2006, pp. 1-3.
18. Smith, Ralph C., *Smart material systems: Model development*, Society of Industrial and Applied Mathematics, Philadelphia, 2005.
19. Jiles, D.C., Thoelke, J.B., Devine, M.K., "Numerical determination of hysteresis parameters for the modeling of magnetic properties using the theory of ferromagnetic hysteresis", IEEE Transactions on Magnetics, vol. 28, No. 1, 1992, pp. 27-35.
20. Jiles, D.C., "A self consistent generalized model for the calculation of minor loop excursions in the theory of hysteresis", IEEE Transaction on Magnetics, vol. 28, No. 5, September 1992, pp. 2602-2604.
21. Carpenter, K.H., "A differential equation approach to minor loops in the Jiles-Atherton hysteresis model," IEEE transactions on magnetics, Vol. 27, No. 6, November 1991, pp. 4404-4406.